Icarus 426 (2025) 116356

Contents lists available at ScienceDirect

Icarus

journal homepage: www.elsevier.com/locate/icarus

Research Paper

Three-dimensional modeling of Ganymede's Chapman–Ferraro magnetic field and its role in subsurface ocean induction

Nawapat Kaweeyanun [a,*], Adam Masters [b]

[a] University of Southampton, School of Physics & Astronomy, Highfield Campus, University Road, Southampton, SO17 1BJ, United Kingdom
[b] Imperial College London, Department of Physics, South Kensington Campus, Exhibition Road, London, SW7 2AZ, United Kingdom

ARTICLE INFO

Dataset link: https://doi.org/10.5258/SOTON/D2542

Keywords:
Ganymede
Magnetospheres
Interiors
Jupiter, satellites

ABSTRACT

In April 2023, the Jupiter Icy Moons Explorer (Juice) began its journey to orbit Jupiter's largest and only magnetic moon, Ganymede. Part of the mission's objectives aim to verify existence of the moon's subsurface ocean and determine its structure through its induced response to external excitation by periodically varying magnetic field. Known contributions to the excitation are those from Jupiter's dipole (at synodic period) and quadrupole (at half-synodic period) variations, and Ganymede's inclined eccentric orbit around Jupiter (at orbital period). We propose that Ganymede's magnetopause, where the Chapman–Ferraro (C–F) magnetic field arises from local currents, also contributes to subsurface ocean induction. This article introduces the first three-dimensional model of the C–F field and its outputs at Ganymede's subsurface ocean and larger magnetosphere. The field is shown to be non-uniform — strongest near upstream Ganymede's subflow region and gradually weakening away from it. Magnetopause asymmetry due to the Jovian guide field results in largely synodic variation of the C–F field, with exceptions near Ganymede's equator and subflow meridian where asymmetry effects are minimal and the variations are half-synodic. The C–F field amplitude is of general order ~ 50 nT, which is significant relative to excitation from the Jovian field. Comparisons to Galileo data and magnetohydrodynamic simulation results suggest the model is useful, therefore the magnetopause effects must be considered in future induction modeling of Ganymede's subsurface ocean ahead of the Juice mission.

1. Introduction

Born with a molten iron core, Ganymede is the only known permanently magnetic satellite in the Solar System (Gurnett et al., 1996; Kivelson et al., 1996; Schubert et al., 1996). The primary Ganymedean dipole magnetic field is ~ 7 times stronger than the ambient Jovian field, affording the moon a distinct magnetosphere (Kivelson et al., 1997, 1998, 2002). Surrounded by Jupiter's plasma at all times, plasma inside Ganymede's magnetosphere follow a Dungey-like convection cycle, driven by frequent and dominant magnetic reconnection on the upstream magnetopause (e.g., Collinson et al., 2018; Jia et al., 2010; Kaweeyanun et al., 2020, 2021).

Jupiter's magnetic field and plasma conditions upstream of Ganymede depend on the moon's absolute latitude relative to (i.e., distance from) the centrifugal equator of the Jovian plasma sheet (Kaweeyanun et al., 2020). In Ganymede's rest frame, this latitude varies at Jovian half-synodic period (5.27 h), resulting in similar periodic oscillation of the upstream conditions. This is noteworthy as the moon contains a conducting subsurface ocean (Kivelson et al., 2002; Saur et al., 2015), and periodic external magnetic excitation of the ocean will induce a magnetic response at amplitude dependent on the liquid layer's thickness, conductivity, and depth from the surface. Study of the ocean's unknown structure via induction is called magnetic sounding, commonly presented as response contour maps seen not only for Ganymede (Seufert et al., 2011; Vance et al., 2021), but also for Europa and Callisto where subsurface oceans are similarly expected (e.g., Zimmer et al., 2000).

Existing magnetic sounding studies utilize numerical multi-shell models that compute oceanic responses to inputs of excitation magnetic fields at several periods. For Ganymede, excitation commonly occur at (but are not limited to) Jovian synodic (10.53 h), Jovian half-synodic, and Ganymedean orbital periods (171.57 h). The first two periods arise from variations of first (dipole) and second (quadrupole) harmonics of the Jovian field, while the third period is due to the moon's orbital inclination and eccentricity. Estimated peak excitation amplitudes of the Jovian field experienced by the moon's subsurface ocean are 84.30 nT, 3.64 nT, and 1.28 nT for synodic, half-synodic, and orbital periods respectively (Vance et al., 2021).

* Corresponding author.
E-mail addresses: N.Kaweeyanun@soton.ac.uk (N. Kaweeyanun), a.masters@imperial.ac.uk (A. Masters).

https://doi.org/10.1016/j.icarus.2024.116356
Received 2 August 2024; Received in revised form 7 October 2024; Accepted 19 October 2024
Available online 28 October 2024
0019-1035/© 2024 The Authors. Published by Elsevier Inc. This is an open access article under the CC BY license (http://creativecommons.org/licenses/by/4.0/).

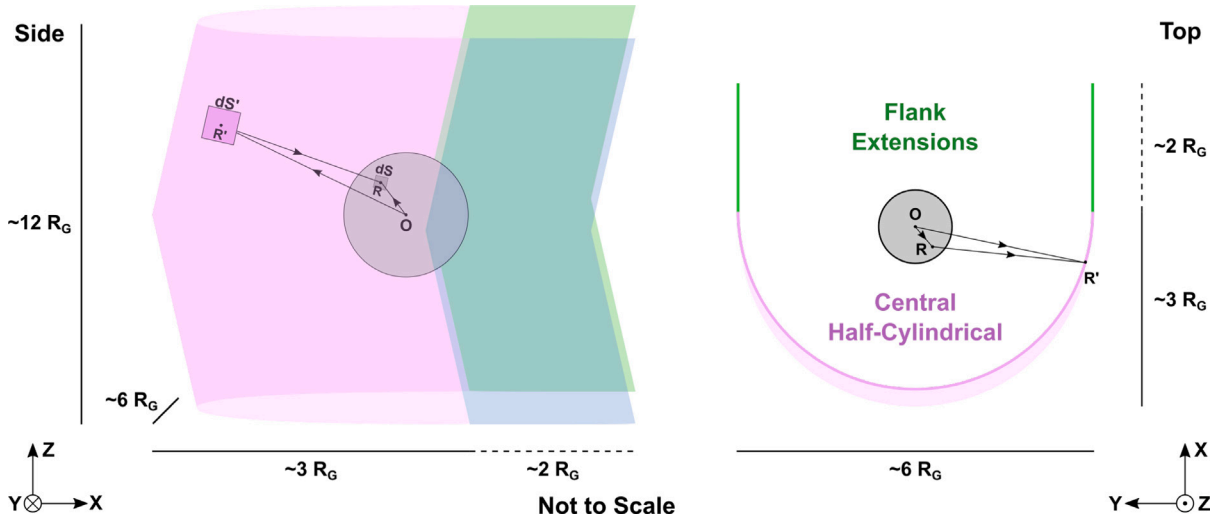

Fig. 1. Schematic diagrams of Ganymede's magnetopause divided into central half-cylindrical (purple) and flank (green) components viewed from the side (left) and from above (right). An illustration of Biot–Savart integration for the Chapman–Ferraro magnetic field experienced by the subsurface ocean is shown. For exact dimensions of the magnetopause model, see text. (For interpretation of the references to color in this figure legend, the reader is referred to the web version of this article.)

However, the current paradigm does not take into account the existence of Ganymede's permanent magnetic field. Magnetic gradient at the moon's upstream magnetopause generates the Chapman–Ferraro (C–F) current (Chapman and Ferraro, 1940), which then via Ampére law produces the C–F magnetic field that compresses the magnetosphere. As the upstream Jovian magnetic field varies half-synodically, one also expects a periodic C–F magnetic field varying around the subsurface ocean. If this is the case, and if the C–F field is significant in amplitude relative to that of Jupiter's magnetic field, then inductive effects of the C–F field will be non-trivial and must be added to current induction models. This will in turn generate a new response contour plots for Ganymede's subsurface ocean before arrival of the Jupiter Icy Moons Explorer (Juice) arrived at Ganymede (Grasset et al., 2013).

The aim of this article is to establish the C–F magnetic field as a non-trivial factor in subsurface ocean induction. For the first time, the C–F field is modeled at Ganymede using a three-dimensional analytical framework (Section 2). The field outputs are then analyzed at Ganymede's subsurface ocean (Section 3) and in the larger magnetosphere (Section 4). Finally, we compare amplitude of the C–F field variation to that of the Jovian magnetic field and establish the non-triviality of the former, and briefly discuss how the two fields' inductive contributions may be separated from Juice data (Section 5).

2. Three-dimensional Chapman–Ferraro magnetic field model

Fig. 1 shows multi-view schematic diagrams of Ganymede's upstream magnetopause in a moon-centered Cartesian coordinate system (GphiO) where X is parallel to Jovian plasma inflow, Y points from Ganymede to Jupiter, and Z is parallel to Jupiter's (and approximately Ganymede's) rotation axis. The central half-cylindrical section of the magnetopause (purple) was first described in Kivelson et al. (1998) and adapted to GphiO coordinates in Kaweeyanun et al. (2020) where the parametrizations were fully detailed. The boundary was fitted to Galileo spacecraft flyby measurements and contained a line of discontinuity along Jupiter's centrifugal equator plane ($Z = 0$) due to presence of modulus in the parametrizing equations.

Our model defines the central magnetopause as a net of square grid elements dS' at position $\boldsymbol{R}$' with 0.05 R_G resolution (where $R_G = 2634$ km is the radius of Ganymede). Grid center points are located between $-14.975\ R_G < Y < 14.975\ R_G$ and $-5.975\ R_G < Z < 5.975\ R_G$ in GphiO coordinates, allowing the equator discontinuity to be hidden exactly along grid edges. The ranges of Y and Z ensure that the magnetopause is always captured at full width, and that no high-latitude contribution is omitted when the C–F magnetic field is later integrated.

As the half-cylindrical description of the magnetopause only extends to $X \sim 0.5\ R_G$, it cannot sufficiently capture C–F currents in the magnetotail. To rectify this issue, the magnetopause is linearly extrapolated in the flank regions (green in Fig. 1) at each latitude Z using final gradients (in the X-Y plane) from the half-cylindrical section. Each flank extension iterates 40 steps at 0.05 R_G, which hides not only the equator discontinuity, but also the discontinuities between central and flank magnetopause sections.

This analytical magnetopause description assumes a smooth surface with no transient interactions (e.g., magnetic reconnection). The boundary is also fixed along the plasma inflow direction (GphiO-X), but can twist along the Jupiter-directed axis (GphiO-Y) with changes in upstream Jovian plasma sheet conditions, which are defined such that

$$\rho_{J,0} = \left(\rho_{J,0}\right)_{\lambda_{III}=248^\circ} e^{\left(\frac{-d}{H}\right)^2} \tag{1}$$

$$P_{J,0} = \left(P_{J,0}\right)_{\lambda_{III}=248^\circ} e^{\left(\frac{-d}{H}\right)^2} \tag{2}$$

$$B_{J,0} = \left|35 sin(\lambda_{III} - 248^\circ)\right| + \left(B_{J,0}\right)_{\lambda_{III}=248^\circ} \tag{3}$$

where $\rho_{J,0}$, $P_{J,0}$, and $B_{J,0}$ are upstream plasma density, (combined thermal and energetic) plasma pressure, and magnetic field strength. $H = \frac{1.62}{\sqrt{ln2}}\ R_J$ is the plasma sheet's scale height ($R_J = 69{,}911$ km), and d is Ganymede's latitude inside the sheet defined by the Jovian System-III east longitude λ_{III} such that in R_J

$$d = \left(15 R_J\right) sin(6.3^\circ) sin(\lambda_{III} - 248^\circ) \tag{4}$$

From Eq. (4), one obtains three key System-III east longitude values: $\lambda_{III} = 248^\circ$ (or equivalently $\lambda_{III} = 68^\circ$) when Ganymede is at the plasma sheet's equator, alongside $\lambda_{III} = 158^\circ$ and $\lambda_{III} = 338^\circ$ when Ganymede is at highest and lowest latitudes inside the sheet respectively. Conditions at the plasma sheet's equator are defined in Eq. (1)–(3) where $\left(\rho_{J,0}\right)_{\lambda_{III}=248^\circ} = 56$ amu/cm^3, $\left(P_{J,0}\right)_{\lambda_{III}=248^\circ} = 3.8$ nPa, and $\left(B_{J,0}\right)_{\lambda_{III}=248^\circ} = 70$ nT. Further away from the equator, plasma density and pressure decrease while magnetic field strength increases. These parametrizations follow results from Jia et al. (2008) in Ganymede's rest frame which takes into account the moon's (relatively slow) orbital motion, therefore the relationship between d and λ_{III} is accurate. The upstream Jovian magnetic field is assumed to have negligible

along plasma inflow direction, and the other two components are approximated such that in nT (Kaweeyanun et al., 2020)

$$B_{J,0,y=-84sin(\lambda_{III}-248°)} \tag{5}$$

$$B_{J,0,z=3cos(\lambda_{III}-248°)-79} \tag{6}$$

The idealized Jovian field is thus restricted to clock angles $\theta_{cl} = 135°–225°$ in the Y-Z plane at the magnetopause subflow point. The model accounts for plasma and magnetic compression near the boundary, total (plasma, magnetic, and dynamic) pressure and field direction. Then, by computing total acting pressure on the boundary, local Ganymede's magnetic field can be calculated assuming cold magnetospheric plasma. For full details, see Kaweeyanun et al. (2020).

Using the magnetopause surface established, one calculates the C–F current at each grid element dS' by Glassmeier et al. (2007b,a)

$$\boldsymbol{j}_{CF} = -\frac{1}{\mu_0}\left[(\boldsymbol{B}_G - \boldsymbol{B}_J)\times \boldsymbol{N}\right] \tag{7}$$

where $\boldsymbol{B}_G$ and $\boldsymbol{B}_J$ are the adjacent Ganymede's and Jupiter's magnetic fields, $\boldsymbol{N}$ is the local magnetopause normal vector pointing toward Ganymede from the magnetopause, and $\mu_0 = 4\pi \times 10^{-7}$ H/m is the permeability of free space.

A measurement point at position $\boldsymbol{R}$ will experience the C–F magnetic field summed across the entire magnetopause. For this, we use Biot–Savart integration

$$\boldsymbol{B}_{CF} = \frac{\mu_0}{4\pi}\iint_{S'} \frac{\boldsymbol{j}_{CF}\times(\boldsymbol{R}-\boldsymbol{R}')}{|\boldsymbol{R}-\boldsymbol{R}'|^3} dS' \tag{8}$$

Fig. 1 shows a measurement point at the topmost boundary of Ganymede's subsurface ocean, defined as a sphere of radius $R_{sp} = 0.95\ R_G$. This translates to a depth of $\sim$ 130 km beneath Ganymede's surface, consistent with an estimate based on the melting curve of pure water (Kivelson et al., 2002). The sphere is discretized into a curvilinear grid at $\Delta\Lambda = 1°$ latitude and $\Delta\phi = 2°$ longitude resolutions, the latter of which increases eastward from the Jupiter-facing prime meridian. Ganymede's ionosphere and outer ice shell are assumed to have negligible impacts on magnetic diffusion between the magnetopause and the ocean sphere.

3. Chapman–Ferraro magnetic field seen by Ganymede's subsurface ocean

Fig. 2 shows by column the C–F magnetic field on Ganymede's top-of-ocean sphere at three main Ganymede positions within the Jovian plasma sheet. When the moon is at the sheet's equator, its magnetopause is symmetric north and south of Ganymede's equator. When the moon is highest or lowest inside the sheet, its magnetopause has maximum north–south asymmetry. The three positions together capture a horizontal 'oscillation' of maximum C–F field amplitudes about the subflow measurement point — defined at $(\Lambda, \phi) = (0°, -90°)$ collinear along the GphiO X-axis to the magnetopause subflow point ($Y = 0$, $Z = 0$).

When $\lambda_{III} = 248°$, the C–F field measures 58.52 nT at the subflow measurement point. This is the maximum amplitude as the field strength decreases monotonically away from this point. The field reaches its minimum amplitude of 5.17 nT at points $(\pm 12.5°, 90°)$, both of which are on the meridian furthest from the magnetopause. The C–F field direction is strongly northward throughout the measurement sphere, enhancing Ganymede's northward internal magnetic field.

Ganymede's northern magnetopause tilts toward Jupiter when the moon is above the plasma sheet's equator and away when the moon is below. Thus, the C–F magnetic field becomes stronger northwest and southeast (southwest and northeast) of the subflow measurement point when $\lambda_{III} = 158°$ ($\lambda_{III} = 338°$). In these two maximum asymmetry cases, the C–F field has identical peak amplitudes of 63.02 nT, but peak locations are reflections across the subflow meridian: $(4°, -78°)$ for $\lambda_{III} = 158°$ and $(4°, -102°)$ for $\lambda_{III} = 338°$. The field minimums meanwhile are 22.86 nT, reached at $(45°, 136°)$ for $\lambda_{III} = 158°$ and $(-45°, 136°)$ for $\lambda_{III} = 338°$. The minimum amplitude is much higher than that of the symmetric case because C–F current contributions north and south of Ganymede's equator do not cancel. The C–F field maintains a northward direction and enhances Ganymede's internal magnetic field.

Non-uniformity of the C–F magnetic field means that subsurface ocean excitation will depend on the point of measurement. Fig. 3 shows evolution of the C–F field strength over one Jovian synodic period, or equivalently $0° \le \lambda_{III} \le 360°$. The field is recorded at $\Delta\lambda_{III} = 2°$ intervals at combination of latitudes $\Lambda = 0°, \pm 35°, \pm 55°, \pm 90°$ and longitudes $\phi = 0°, 90°, 180°, -90°$ on the 0.95 R_G top-of-ocean sphere.

Consider first at Ganymede's equator ($\Lambda = 0°$, Fig. 3a), the C–F field amplitudes vary at half-synodic period at all longitudes, with minimums when Ganymede is $|\Delta\lambda_{III}| \sim 20°$ from the Jovian plasma sheet equator, and maximums when the moon is highest and lowest inside the sheet. The minimums and the maximums correspond respectively to maximums and minimums of Jovian pressure acting on the magnetopause. The acting pressure is not at minimum when Ganymede is at plasma sheet equator due to competing influences between Jovian magnetic and plasma/dynamic pressures, which decrease and increase with the moon's distance from the sheet equator respectively. Local fluctuations between C–F field minimum and maximum amplitudes are attributed to the evolving magnetopause structure. Small troughs uniquely seen at anti-subflow point ($\phi = 90°$) at sheet-center longitudes are likely products of idealized magnetopause description. The ranges between minimum and maximum B_{CF} values i.e., field variation extent, are 26.95 nT, 21.39 nT, 26.95 nT and 14.71 nT for $\phi = 0°, 90°, 180°, -90°$ respectively. As expected, the field is strongest at subflow measurement point, weakest at anti-subflow measurement point $(0°, 90°)$, with intermediate values at flank measurement points.

Next we move to Ganymede's poles ($\Lambda = \pm 90°$, Fig. 3f–3g) where there is no longitude effect. The C–F field amplitudes here vary identically at north and south poles, exhibiting half-synodic periods with local patterns identical to those at Ganymede's equatorial subflow point. The range of B_{CF} variation is 17.60 nT.

At mid-lower latitudes ($\Lambda = \pm 35°$, Fig. 3b–3c), the C–F field variations at subflow and anti-subflow measurement points are half-synodic with same local patterns as those at Ganymede's equator. The range of B_{CF} variation is 13.74 nT at higher-amplitude the subflow measurement point and 20.08 nT at lower-amplitude anti-subflow point. However, a new pattern emerges when the C–F field is measured at the flanks ($\phi = 0°, 180°$). The variations here are synodic, each consisting of two half-synodic 'half-periods' when Ganymede is above and below the Jovian plasma sheet equator. This is due to the magnetopause tilt. Consider the northern sub-Jovian measurement point ($\Lambda = 35°, \phi = 0°$). It is closer to the magnetopause when Ganymede is northward of the plasma sheet equator and further away when the moon is southward of the equator. Hence, the C–F field when $\lambda_{III} = 158°$ is stronger than when $\lambda_{III} = 338°$, because the former 'half-period maximum' occurs when the moon is closer to the magnetopause than the latter. Meanwhile, the southern sub-Jovian measurement point ($\Lambda = 35°, \phi = 180°$) exhibits a reflected pattern where 'half-period maximum' is stronger when $\lambda_{III} = 338°$, because it experiences the opposite magnetopause tilt over the synodic period. Further reflections apply for southern flank measurement points. The sub-Jovian southern point will experience variation identical to the anti-Jovian northern point and vice versa. Within each 'half-period', variation follows the pattern described at Ganymede's equator, and the B_{CF} range at each flank measurement point is 32.55 nT.

Finally, mid-higher latitudes ($\Lambda = \pm 55°$, Fig. 3e–3f) experience variations similar to those at mid-lower latitudes, with half-synodic variations along the subflow great circle and synodic variations at the flanks. The ranges of B_{CF} at mid-higher latitudes are 28.43 nT, 19.84 nT, 28.43 nT, 14.94 nT at $\phi = 0°, 90°, 180°, -90°$ respectively.

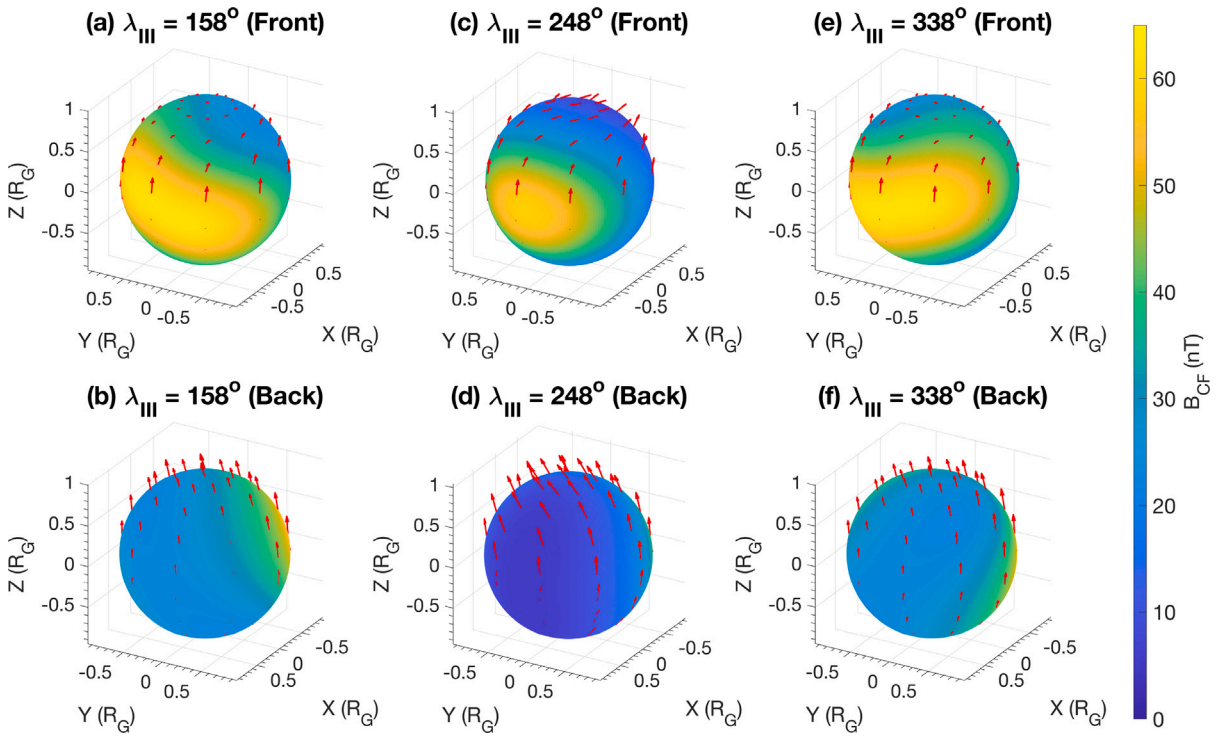

Fig. 2. The C–F magnetic field strength and direction experienced by the top-of-ocean sphere when Ganymede is at its highest (a–b), equatorial (c–d), and lowest (e–f) positions in the Jovian plasma sheet. Top and bottom rows show upstream and downstream views of the sphere respectively. Magnetic field points in direction of the red arrows. (For interpretation of the references to color in this figure legend, the reader is referred to the web version of this article.)

It is arguable that half-synodic variations are merely product of an idealized model, and in reality there exists no points at which the magnetopause tilt effect is negligible. However, the C–F magnetic field variation will be close to half-synodic along Ganymede's equator and its subflow great circle, and therefore the period should not be discounted entirely. At other locations, however, one should expect the C–F field to vary synodically with smaller discrepancies between the two 'half-periods' than at sub-Jovian or anti-Jovian points.

The C–F magnetic field has so far been measured on the $R_{sp} = 0.95\ R_G$ top-of-ocean sphere. However, by adjusting the sphere's radius, the field can be measured at any depth inside Ganymede. This allows the impact of uncertain subsurface ocean location to be evaluated. Fig. 4 shows the C–F magnetic field strength measured at the subflow measurement points across sphere radius range $R_{sp} = 1.00$–$0.00\ R_G$ at $0.05\ R_G$ interval. Here B_{CF} varies identically at northern and southern latitudes as these points do not experience magnetopause asymmetry, so only the former is shown.

The original measurement sphere radius is noted at $R_{sp} = 0.95\ R_G$. An estimated boundary between Ganymede's ice shell and silicate mantle i.e., deepest possible ocean depth, is also marked at $R_{sp} = 0.70\ R_G$. The C–F magnetic field generally decreases in strength with decreasing radius as the sphere shrinks away from the magnetopause. The only exception is at the poles, where shrinkage brings the measurement points closer to equator where the C–F field is stronger. The pattern is the same whether Ganymede is at Jovian plasma sheet equator (Fig. 4a) or at highest/lowest in-sheet latitudes (Fig. 4b). At viable ocean depths, B_{CF} always remains above 35 nT at non-polar locations, suggesting that a deeper ocean will not eliminate excitation from the C–F magnetic field.

4. Chapman–Ferraro magnetic field in Ganymede's magnetosphere

As Eq. (8) imposes no restriction on measurement point position, our C–F magnetic field model can in fact be applied to all of Ganymede's magnetosphere. Each subplot in Fig. 5 utilizes a measurement plane defined between $-2.0\ R_G < X < 2.0\ R_G$ and $-2.0\ R_G < Y < 2.0\ R_G$ with $0.05\ R_G$ resolution. The plane can be fixed at a constant $Z = Z_0$ latitude i.e., it represents a horizontal cross section of Ganymede's magnetosphere.

Fig. 5a–5c demonstrate the C–F magnetic field at Ganymede's equator for the three main Ganymede positions within the Jovian plasma sheet. At each Ganymede position, the equatorial magnetopause is equidistant to the moon on sub-Jovian and anti-Jovian flanks, therefore reduction of B_{CF} from the boundary to Ganymede occurs at equal rate. Comparison between Ganymede positions show slight moonward shift of the magnetopause when the moon is highest/lowest in the plasma sheet, increasing the C–F field strength in the upstream region.

In the northern magnetosphere ($Z > 0\ R_G$), the magnetopause will be closer to Ganymede on the sub-Jovian flank ($Y > 0\ R_G$) and further away on the anti-Jovian flank ($Y < 0\ R_G$), resulting in stronger and weaker C–F magnetic field respectively when Ganymede is northward of the plasma sheet equator. If Ganymede is southward, then the enhancement pattern will reverse. Further reflections apply in the southern magnetosphere ($Z < 0\ R_G$), where B_{CF} will be stronger on the anti-Jovian flank when Ganymede is northward of the plasma sheet equator, and stronger on the sub-Jovian flank when the moon is southward of the equator. These patterns become evident by comparing Fig. 5d and Fig. 5h. The two cross sections were at almost exactly opposite magnetospheric latitudes Z_0 when Ganymede is at opposite latitudes in the Jovian plasma sheet. As the result, they exhibit nearly identical C–F magnetic field inside the magnetosphere with enhancement seen on the sub-Jovian flank.

Strength of the C–F field experienced at a point in Ganymede's magnetosphere is dictated primarily by its distance from the magnetopause. In the closed field region ($|Z| < 0.63\ R_G$), the field amplitude approaches 100 nT near the upstream boundary and decreases toward the downstream. The magnetopause flanks meanwhile has B_{CF} of order ~ 30–50 nT, though it can be stronger if the tilted boundary is nearby, and in the wake region the C–F field strength reduces to less than 10

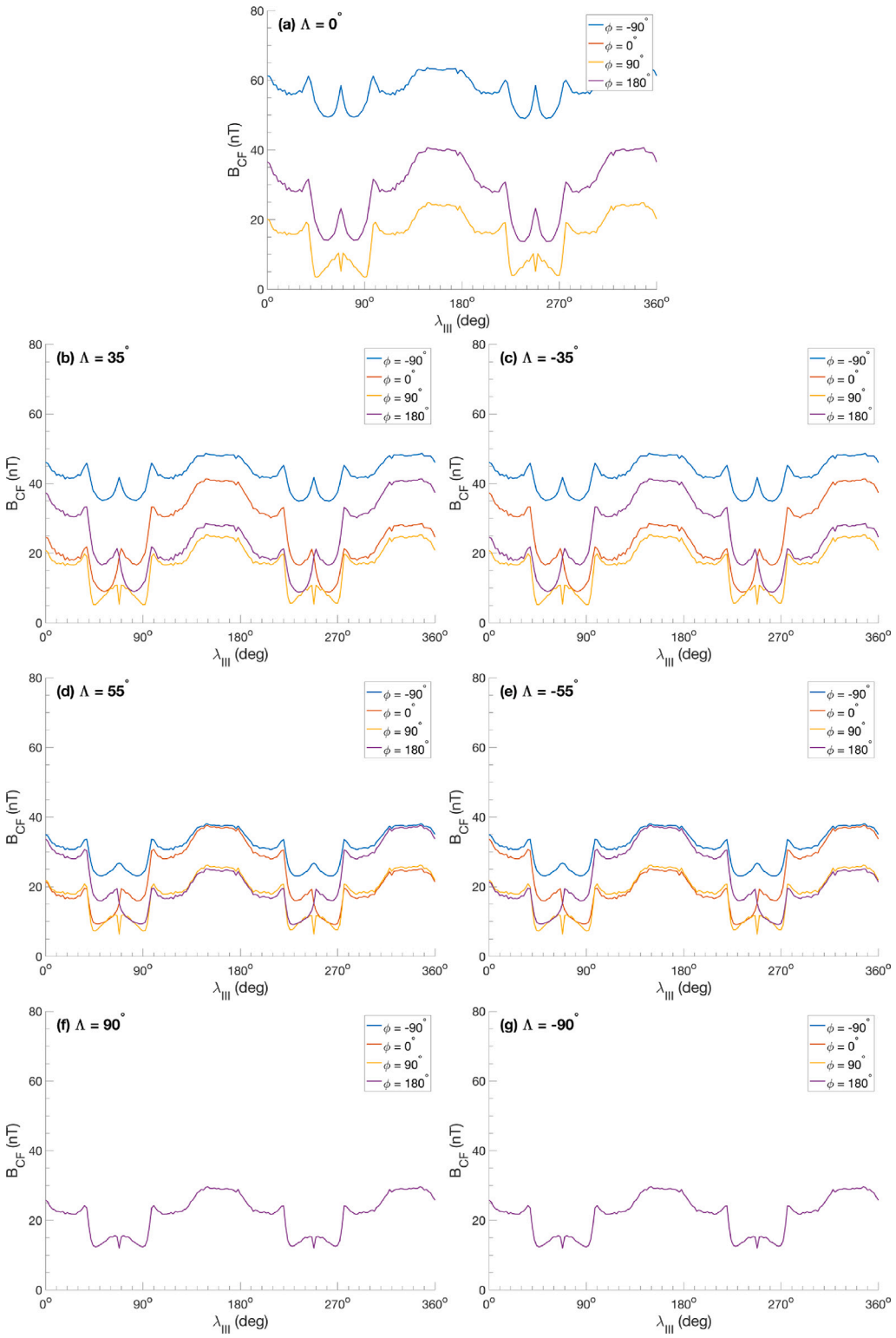

Fig. 3. The C–F magnetic field strength measured over one Jovian synodic period across combination of latitudes and longitudes on Ganymede's top-of-ocean sphere. Each subplot corresponds to a single latitude with all longitudes shown. (For interpretation of the references to color in this figure legend, the reader is referred to the web version of this article.)

nT. In the open field region ($|Z| > 0.63\ R_G$), the C–F field becomes substantially weaker across the magnetosphere, which is expected as the C–F current is much stronger in the closed-field region where Jupiter's and Ganymede's magnetic fields are anti-parallel.

Another motivation for the magnetospheric C–F field study is model evaluation. Fig. 5d–5i are in fact chosen for consistency with the Galileo spacecraft's six flybys of Ganymede — denoted *G*1, *G*2, *G*7, *G*8, *G*28, and *G*29 as red dots in the subplots. We identify the times when Galileo was in the sub-Jovian flank at $Y = 1.5\ R_G$ (*G*2 and *G*7), the anti-Jovian flank at $Y = -1.5\ R_G$ (*G*1 and *G*29), and the upstream magnetopause at $Y = 0\ R_G$ (*G*8 and *G*28), then obtain corresponding Z_0 and λ_{III} values.

However, Galileo's magnetic field data is a total of multi-source contributions, from Ganymede's permanent internal field to Jupiter's ambient magnetic field, to induced field of the subsurface ocean and

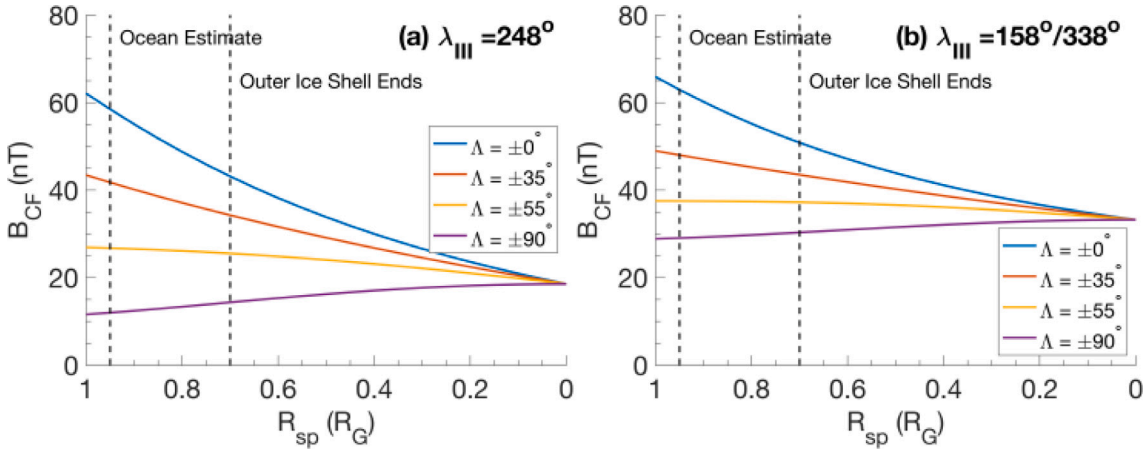

Fig. 4. The C–F magnetic field strength as a function of depth inside Ganymede when the moon is at (a) equatorial and (b) highest/lowest positions inside the Jovian plasma sheet. The estimated boundary between Ganymede's ice shell and silicate mantle — upper limit to depth of subsurface ocean is denoted by the vertical dashed line. (For interpretation of the references to color in this figure legend, the reader is referred to the web version of this article.)

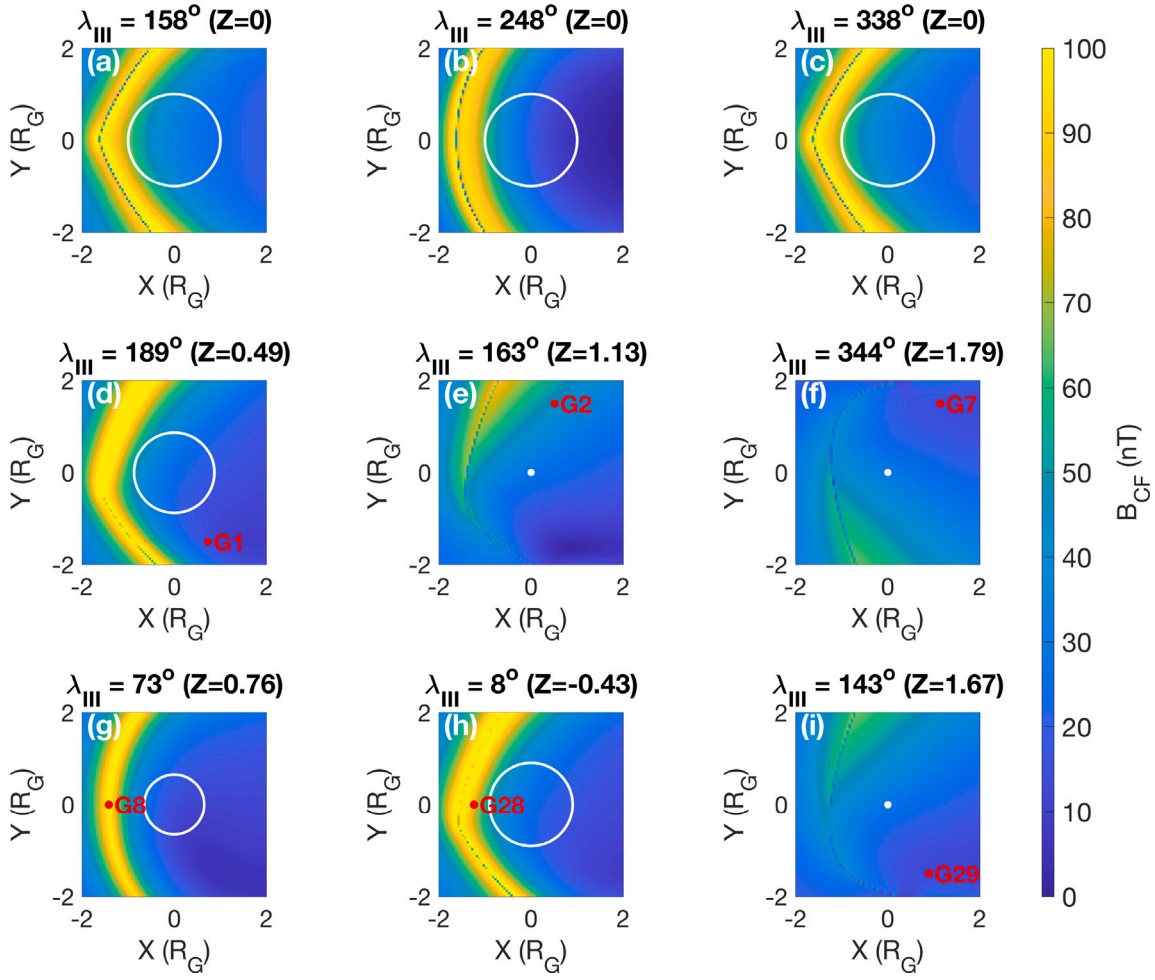

Fig. 5. The C–F magnetic field strength across Ganymede-centered 4 $R_G \times 4R_G$ planes at (a–c) Ganymede's equator for extreme Jovian System-III east longitudes and (d–f) $Z = Z_0$ Rt_G latitudes and System-III east longitudes matching the six Galileo flybys of Ganymede. (For interpretation of the references to color in this figure legend, the reader is referred to the web version of this article.)

fields of external currents surrounding the moon. An attempt has been made to isolate magnetic field contribution of currents by subtracting from Galileo data numerical magnetohydrodynamic (MHD) model outputs containing all non-current fields (Olsen et al., 2010). The study focuses in particular the G2 and the G28 flybys, with more detailed results available for the latter. From Figure 7 in Olsen et al. (2010), one obtains a currents' field of (21, −10, 62) nT in GphiO coordinates at 20 May 2000, 10:10 UT, when Galileo is approximately at location in Fig. 5h. Our analytical C–F magnetic field here is (38, −23, 66) nT. Because Galileo was very close to the upstream magnetopause in the closed-field region, the C–F current was strongly dominant over all other currents (magnetotail, Alfvén wing, etc.), so comparison between the two magnetic fields is relatively like-to-like. The fields are similar in their dominant Z-components, but the analytical model predicts stronger X and Y components by a roughly a factor of two thus a $\sim 20\%$ stronger magnetic field strength (80 nT vs 66 nT).

If contributions of other currents were truly negligible, then discrepancies between the two fields likely come down to model differences. The analytical model enforces a dependent relationship between Ganymede's and Jupiter's magnetic fields to fix the magnetopause location. In contrast, Ganymede's and Jupiter's fields are independent in the numerical MHD model and the magnetopause position is derived more realistically from pressure balance. Olsen et al. (2010), however, separated current and non-current magnetic fields using spacecraft trajectories — a highly approximative method that can inaccurately divide contributions. These modeling differences, in addition to inputs used, affect comparison between the two models. Nevertheless, similarities between their results suggest a measure of usefulness for our analytical model.

5. Discussion

For the first time, the Chapman–Ferraro (C–F) magnetic field is described in three dimensions based on parametrizations of Ganymede's magnetopause and the upstream Jovian plasma sheet. The analytical model is capable of tracking C–F field evolution and has been computed at Ganymede's conducting subsurface ocean, where magnetic induction is expected, and at cross sections of the moon's magnetosphere, predicting the C–F field's impacts at global scale.

The amplitude of C–F field inside Ganymede's magnetosphere is of order $\sim 10^1$ nT. The magnetopause field is highly non-uniform and varies periodically. At the subsurface ocean, the C–F field's amplitude at Jovian synodic period ($\sim$ 20–40 nT) is significant relative to that of the Jovian dipole field (84.3 nT), while at half-synodic period the C–F field ($\sim$ 20–60 nT) is dominant over that of the Jovian quadrupole field (3.64 nT). The presence of Ganymede's permanent magnetic field is therefore of consequence to induction in the moon's subsurface ocean.

Our analytical model results are comparable to those from numerical magnetohydrodynamic simulations that separate currents' magnetic field contribution from Galileo flybys (Olsen et al., 2010). General accuracy of the analytical model is important as its efficiency allows readily application, which is useful given scarcity of observational data before the Jupiter Icy Moons Explorer (Juice).

In addition to its enforced magnetopause location discussed in Section 4, the analytical model has thus far assumed smooth periodic variations of conditions in the Jovian plasma sheet. For a more realistic depiction of the non-uniform sheet, random fluctuations can be simulated through more complex condition functions or direct adjustments to the condition arrays at the Jovian-side magnetopause, either by randomization or empirical inputs once measurement data become available. Fortunately, plasma sheet fluctuations typically occur over timescales of weeks (Bagenal et al., 2016), so within a synodic period variations of the upstream conditions should be close to idealized dictated by Ganymede's steady in-sheet trajectory. Our current analysis is intended as a discussion starter, and the model can be adjusted to meet future needs in a more case-specific basis.

Inclusion of the C–F magnetic field into forward induction models (e.g., Styczinski et al., 2022, 2023) is the next step along this research avenue. The C–F field variations will combine with those from the Jovian field at the same periods, resulting in new predictions for the subsurface ocean's inductive response and structure, both of which will be verified upon arrival of Juice at Ganymede. Separating contributions from the two non-uniform magnetic fields will be a complex task especially from spacecraft measurement data. One possible method is Principal Component Analysis (PCA), which reorganizes magnetic time-series data into subspace defined by axes of maximum variance (Cochrane et al., 2022). The procedure should amplify contribution from the C–F field, which can then be distinguished once compared to forward modeled inductive responses with and without magnetopause excitation. Fully conducting this analysis, however, is beyond the scope of this article.

CRediT authorship contribution statement

Nawapat Kaweeyanun: Writing – original draft, Visualization, Software, Methodology, Investigation, Formal analysis, Data curation, Conceptualization. **Adam Masters:** Writing – review & editing, Validation.

Declaration of competing interest

The authors declare that they have no known competing financial interests or personal relationships that could have appeared to influence the work reported in this paper.

Acknowledgments

N. Kaweeyanun is supported by the Science and Technology Facilities Council (STFC) Consolidated Grant (ST/V000942/1). A. Masters is supported by a Royal Society University Research Fellowship.

Data availability

Derived data used in Figs. 2–5 is available from the University of Southampton Institutional Research Repository at Kaweeyanun (2024), or at https://doi.org/10.5258/SOTON/D2542.

References

Bagenal, F., Wilson, R.J., Siler, S., Paterson, W.R., Kurth, W.S., 2016. Survey of Galileo plasma observations in jupiter's plasma sheet. J. Geophys. Res.: Planets 121 (5), 871–894. http://dx.doi.org/10.1002/2016JE005009.

Chapman, S., Ferraro, V.C.A., 1940. The theory of the first phase of a geomagnetic storm. Terr. Magn. Atmos. Electr. 45 (3), 245–268. http://dx.doi.org/10.1029/TE045i003p00245.

Cochrane, C.J., Persinger, R.R., Vance, S.D., Midkiff, E.L., Castillo-Rogez, J., Luspay-Kuti, A., Liuzzo, L., Paty, C., Mitchell, K.L., Prockter, L.M., 2022. Single- and multi-pass magnetometric subsurface ocean detection and characterization in icy worlds using principal component analysis (PCA): Application to triton. Earth Space Sci. 9 (2), e2021EA002034. http://dx.doi.org/10.1029/2021EA002034.

Collinson, G., Paterson, W.R., Bard, C., Dorelli, J., Glocer, A., Sarantos, M., Wilson, R., 2018. New results from Galileo's first flyby of Ganymede: Reconnection-driven flows at the low-latitude magnetopause boundary, crossing the cusp, and icy ionospheric escape. Geophys. Res. Lett. 45 (8), 3382–3392. http://dx.doi.org/10.1002/2017GL075487.

Glassmeier, K.H., Auster, H.U., Motschmann, U., 2007a. A feedback dynamo generating mercury's magnetic field. Geophys. Res. Lett. 34 (22), http://dx.doi.org/10.1029/2007GL031662.

Glassmeier, K.H., Grosser, J., Auster, U., Constantinescu, D., Narita, Y., Stellmach, S., 2007b. Electromagnetic induction effects and dynamo action in the hermean system. Space Sci. Rev. (2), 511–527. http://dx.doi.org/10.1007/s11214-007-9244-9.

Grasset, O., Dougherty, M.K., Coustenis, A., Bunce, E., Erd, C., Titov, D.V., Blanc, M., Coates, A., Drossart, P., Fletcher, L., Hussmann, H., Jaumann, R., Krupp, N., P. Lebreton, J., Prieto-Ballesteros, O., Tortora, P., Tosi, F., Van Hoolst, T., 2013. JUpiter ICy moons Explorer (JUICE): An ESA mission to orbit Ganymede and to characterise the jupiter system. Planet. Space Sci. 78, 1–21. http://dx.doi.org/10.1016/j.pss.2012.12.002.

Gurnett, D.A., Kurth, W.S., Roux, A., Bolton, S.J., Kennel, C.F., 1996. Evidence for a magnetosphere at Ganymede from plasma-wave observations by the Galileo spacecraft. Nature 384 (6609), 535–537. http://dx.doi.org/10.1038/384535a0.

Jia, X., Walker, R.J., Kivelson, M.G., Khurana, K.K., Linker, J.A., 2008. Three-dimensional MHD simulations of Ganymede's magnetosphere. J. Geophys. Res. Space Phys. 113 (A6), http://dx.doi.org/10.1029/2007JA012748.

Jia, X., Walker, R.J., Kivelson, M.G., Khurana, K.K., Linker, J.A., 2010. Dynamics of Ganymede's magnetopause: Intermittent reconnection under steady external conditions. J. Geophys. Res. Space Phys. 115 (A12), http://dx.doi.org/10.1029/2010JA015771.

Kaweeyanun, N., 2024. Dataset: Three-dimensional modeling of Ganymede's Chapman-Ferraro magnetic field and its role in subsurface ocean induction. University of Southampton Repository, https://doi.org/10.5258/SOTON/D2542.

Kaweeyanun, N., Masters, A., Jia, X., 2020. Favorable conditions for magnetic reconnection at Ganymede's upstream magnetopause. Geophys. Res. Lett. 47 (6), e2019GL086228. http://dx.doi.org/10.1029/2019GL086228.

Kaweeyanun, N., Masters, A., Jia, X., 2021. Analytical assessment of Kelvin-Helmholtz instability growth at Ganymede's upstream magnetopause. J. Geophys. Res. Space Phys. 126 (8), e2021JA029338. http://dx.doi.org/10.1029/2021JA029338.

Kivelson, M.G., Khurana, K.K., Coroniti, F.V., Joy, S., Russell, C.T., Walker, R.J., Warnecke, J., Bennett, L., Polanskey, C., 1997. The magnetic field and magnetosphere of Ganymede. Geophys. Res. Lett. 24 (17), 2155–2158. http://dx.doi.org/10.1029/97GL02201.

Kivelson, M.G., Khurana, K.K., Russell, C.T., Walker, R.J., Warnecke, J., Coroniti, F.V., Polanskey, C., Southwood, D.J., Schubert, G., 1996. Discovery of Ganymede's magnetic field by the Galileo spacecraft. Nature 384 (6609), 537–541. http://dx.doi.org/10.1038/384537a0.

Kivelson, M.G., Khurana, K.K., Volwerk, M., 2002. The permanent and inductive magnetic moments of Ganymede. Icarus 157 (2), 507–522. http://dx.doi.org/10.1006/icar.2002.6834.

Kivelson, M.G., Warnecke, J., Bennett, L., Joy, S., Khurana, K.K., Linker, J.A., Russell, C.T., Walker, R.J., Polanskey, C., 1998. Ganymede's magnetosphere: Magnetometer overview. J. Geophys. Res.: Planets 103 (E9), 19963–19972. http://dx.doi.org/10.1029/98JE00227.

Olsen, N., Glassmeier, K.H., Jia, X., 2010. Separation of the magnetic field into external and internal parts. Space Sci. Rev. 152 (1), 135–157. http://dx.doi.org/10.1007/s11214-009-9563-0.

Saur, J., Duling, S., Roth, L., Jia, X., Strobel, D.F., Feldman, P.D., Christensen, U.R., Retherford, K.D., McGrath, M.A., Musacchio, F., Wennmacher, A., Neubauer, F.M., Simon, S., Hartkorn, O., 2015. The search for a subsurface ocean in Ganymede with hubble space telescope observations of its auroral ovals. J. Geophys. Res. Space Phys. 120 (3), 1715–1737. http://dx.doi.org/10.1002/2014JA020778.

Schubert, G., Zhang, K., Kivelson, M.G., Anderson, J.D., 1996. The magnetic field and internal structure of Ganymede. Nature 384 (6609), 544–545. http://dx.doi.org/10.1038/384544a0.

Seufert, M., Saur, J., Neubauer, F.M., 2011. Multi-frequency electromagnetic sounding of the Galilean moons. Icarus 214 (2), 477–494. http://dx.doi.org/10.1016/j.icarus.2011.03.017.

Styczinski, M.J., Vance, S.D., Harnett, E.M., Cochrane, C.J., 2022. A perturbation method for evaluating the magnetic field induced from an arbitrary, asymmetric ocean world analytically. Icarus 376, 114840. http://dx.doi.org/10.1016/j.icarus.2021.114840.

Styczinski, M.J., Vance, S.D., Melwani Daswani, M., 2023. PlanetProfile: Self-consistent interior structure modeling for ocean worlds and rocky dwarf planets in python. Earth Space Sci. 10 (8), e2022EA002748. http://dx.doi.org/10.1029/2022EA002748.

Vance, S.D., Styczinski, M.J., Bills, B.G., Cochrane, C.J., Soderlund, K.M., Gómez-Pérez, N., Paty, C., 2021. Magnetic induction responses of jupiter's ocean moons including effects from adiabatic convection. J. Geophys. Res.: Planets 126 (2), e2020JE006418. http://dx.doi.org/10.1029/2020JE006418.

Zimmer, C., Khurana, K.K., Kivelson, M.G., 2000. Subsurface oceans on Europa and Callisto: Constraints from Galileo magnetometer observations. Icarus 147 (2), 329–347. http://dx.doi.org/10.1006/icar.2000.6456.

Nawapat Kaweeyanun is a Research Fellow in Magnetospheric Physics at the University of Southampton. He obtained his Ph.D. in Physics from Imperial College London, where he investigated Ganymede's upstream magnetopause and its driving role for the Solar System's only moon magnetosphere. Since then he has continued to explore the magnetopause's inductive effect on Ganymede's subsurface ocean ahead of the Jupiter Icy Moons Explorer Mission, while expanding his research interest to Earth's auroras, using instrument and image data to capture their impacts on the terrestrial magnetosphere's structure.

Adam Masters is a space and planetary scientist with the Space & Atmospheric Physics Group at Imperial. His research focuses on explaining how energy flows through the Solar System via magnetic fields and charged particle motion in space, as well as understanding how different bodies in the Solar System generate magnetic fields in their interiors. His research programme is underpinned by his involvement in spacecraft missions, such as the Cassini–Huygens mission to Saturn and Titan that ended in September 2017, the Jupiter Icy Moons Explorer mission currently being built for launch, and ongoing high-level planning of future missions to Uranus and Neptune.